Environmental Science & Technology

pubs.acs.org/est

Open Access

This article is licensed under CC-BY-NC-ND 4.0

Article

Anatomy of Summertime Upslope Events in Northeastern Colorado: Ammonia (NH_3) Transport to the Rocky Mountains

Julieta F. Juncosa Calahorrano,* Amy P. Sullivan, Ilana B. Pollack, Joseph R. Roscioli, Megan E. McCabe, Kathryn M. Steinmann, Dana R. Caulton, En Li, Jeffrey R. Pierce, Lillian E. Naimie, Da Pan, Jeffrey L. Collett, Jr., and Emily V. Fischer*

Cite This: *Environ. Sci. Technol.* 2024, 58, 16922−16930

Read Online

ACCESS | Metrics & More | Article Recommendations | Supporting Information

ABSTRACT: The Transport and Transformation of Ammonia (TRANS^{2}Am) airborne field campaign occurred over northeastern Colorado during the summers of 2021 and 2022. A subset of the TRANS^{2}Am flights investigated easterly wind conditions capable of moving agricultural emissions of ammonia (NH_3) through urban areas and into the Rocky Mountains. TRANS^{2}Am captured 6 of these events, unveiling important commonalities. (1) NH_3 enhancements are present over the mountains on summer afternoons when easterly winds are present in the foothills region. (2) The abundance of gas-phase NH_3 is 1 and 2 orders of magnitude higher than particle-phase NH_4^+ over the mountains and major agricultural sources, respectively. (3) During thermally driven circulation periods, emissions from animal husbandry sources closer to the mountains likely contribute more to the NH_3 observed over the mountains than sources located further east. (4) Transport of plumes from major animal husbandry sources in northeastern Colorado westward across the foothills requires ∼5 h. (5) Winds drive variability in the transport of NH_3 into nearby mountain ecosystems, producing both direct plume transport and recirculation. A similar campaign in other seasons, including spring and autumn, when synoptic scale events can produce sustained upslope transport, would place these results in context.

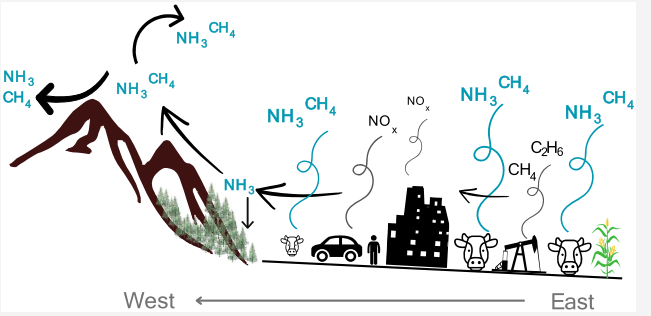

KEYWORDS: *agricultural ammonia, ammonia deposition, sensitive ecosystem, airborne observations*

Downloaded via COLORADO STATE UNIV on October 9, 2024 at 22:04:08 (UTC).
See https://pubs.acs.org/sharingguidelines for options on how to legitimately share published articles.

1. INTRODUCTION

Nitrogen (N) cycling is essential for the biological and chemical processes sustaining life on Earth. The imbalance in the N cycle, caused by a doubling of anthropogenic emissions since the Industrial Revolution, has been identified by the unhealthy accumulation of N in water reservoirs, soils, and, temporarily, in the atmosphere.[1−3] The environmental implications of N emissions, deposition, and accumulation include soil acidification, water eutrophication, and air pollution.[4−7] Over the past decade, reduced forms of N ($NH_x = NH_3 + NH_4^+$) have become the primary source of N-deposition in the U.S. and other regions of the globe.[8,9]

In N-limited ecosystems, such as those in the Western U.S., small increases in N can lead to undesirable environmental impacts. For example, N-deposition in Rocky Mountain National Park (RMNP)[4,5,10−14] has been linked to adverse effects on biological and ecological processes.[6,7,13,15,16] RMNP is located southwest of a large agricultural area extending from the eastern plains to the northern Colorado foothills. Animal feeding operations are a large regional source of reduced N.[17] The eastern side of RMNP experiences N-deposition on days when synoptic (spring/autumn) or thermally driven (summer) upslope winds transport emissions through the urban corridor, the foothills, and into RMNP.[4,18]

N-deposition to RMNP is complex. Peak deposition typically occurs in July.[19,20] Wet deposition of ammonium (NH_4^+) and nitrate (NO_3^-) are the two largest deposition pathways, but dry deposition of ammonia (NH_3) is also significant and highly uncertain.[24] Between 1990 and 2017, inorganic wet N-deposition has been relatively constant, but this is the result of compensating decreases in wet NO_3^- deposition and increases in NH_4^+ wet deposition.[25] Several studies have worked to better document and attribute the sources of N reaching RMNP. Increased chemical tracer concentrations were linked to easterly flow (i.e., upslope winds) in three mountain sites at RMNP.[10] The Rocky Mountain Atmospheric Nitrogen and Sulfur Studies (Ro-

Received: December 30, 2023
Revised: July 31, 2024
Accepted: August 1, 2024
Published: September 11, 2024

© 2024 The Authors. Published by American Chemical Society

MANS) field campaign showed regional gradients of NH_x with higher concentrations near sources (especially east of the park) that decreased toward the mountains.[11] Year-long observations showed that spring and summer are the peak periods for NH_x-deposition in RMNP.[19,20] The critical load of N, defined as the amount of N that leads to harmful changes in an ecosystem,[16] for wet and wet + dry N-deposition in RMNP is 1.5 and 3 kg N ha^{-1} y^{-1}, respectively.[12,16,21] Benedict et al.[11] reported a N-deposition rate of 3.65 kg N ha^{-1} y^{-1} for the RMNP during RoMANS. Other analyses from RoMANS attributed a large percentage (44−56%) of the reduced N observed in RMNP to sources within eastern Colorado during summer.[13,22−24,26] The diurnal cycles of N-containing species in the gas- and particle-phase in RMNP show higher concentrations are often present in the afternoon during the summer.[27] Pan et al.[28] observed higher N-deposition when air masses passed over upwind agricultural regions (7.9 ng m^{-2} s^{-1}) than over urban areas (1 ng m^{-2} s^{-1}). Prior studies support the hypothesis that a large percentage of N-deposition in RMNP can be attributed to emissions from agricultural sources to the east.

We present aircraft observations of NH_x plumes as they travel from the eastern agricultural region across the Colorado Front Range (CFR) urban corridor and into the Rocky Mountains (RM) during summer upslope events. We quantify plume transit times and identify different flow patterns that support the movement of agricultural NH_x plumes into the mountains and their recirculation. We also identify particular regions and facilities with high potential for plume transport into the mountains during summer upslope events.

2. METHODS

2.1. Campaign Overview and Sampling Strategy. TRANS^{2}Am occurred over two phases: (I) July 27 - August 23, 2021, and (II) August 16 - September 02, 2022. During both phases, the University of Wyoming King Air (UWKA) was based at Laramie Regional Airport (KLAR) in Laramie, WY, and deployed to the northern CFR. A mobile lab was also deployed for the sampling of RF21 (see Figure S1 and Text S1). We sampled six upslope events: TF04, RF07, RF10 (Phase I) and RF16, RF18, RF21 (Phase II) (see Table S1). During Phase I the region was impacted by local and transported smoke from fires in the western U.S. (Washington, Oregon, California, and Arizona).[29] This was not the case during Phase II where levels of carbon monoxide (CO) across all flights were lower.

The TRANS^{2}Am sampling strategy included four north−south flight "legs" at two different altitudes (~500−1000 and ~1500−2000 ft agl) and different longitudes across the study region (Figure 1a). The four legs (L1 to L4) were centered at 104.50, 104.84, 105.21, and 105.50°W. L1 and L2 were positioned in the region with the largest number of facilities in the area. The easternmost leg (L1) passed nearby large cattle and dairy facilities (10,000 -> 100,000 hd). L2 was located downwind (west) of the densest concentration of livestock facilities and ~10 km downwind of one of the largest facilities (>100,000 hd) in the area. L3 was located west of the major Colorado urban corridor, including Fort Collins, Loveland, and Longmont. There are 22 animal husbandry facilities between L2 and L3, most of which are dairies with <10,000 hd, except for one sheep farm. Finally, L4 passed over Estes Park, the town directly abutting RMNP to the east. Figure 1b shows an overview of terrain averaged longitudinally (102−106° W),

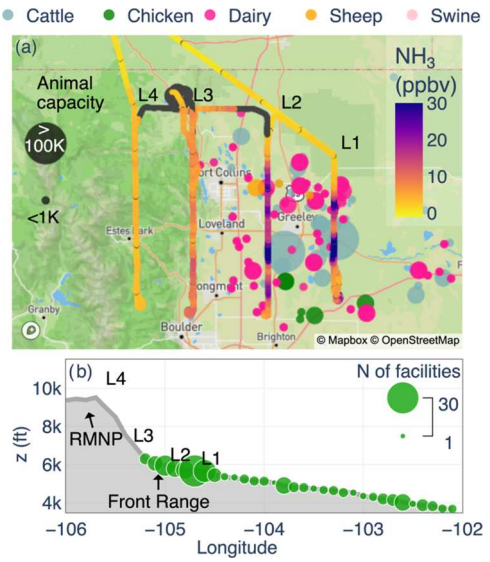

Figure 1. (a) Flight track of the UWKA colored by NH_3 (ppbv) on August 29, 2022 (RF21), between 13:10 and 16:20 LT (MDT). This flight track is representative of sampling during Phase I and Phase II of TRANS^{2}Am under easterly winds. Dots represent agricultural facilities colored by the type of animal and sized by the reported maximum capacity in animal units (hd). (b) Longitudinal average (every 0.1°) of the study region terrain. The size of the green dots represents the number of facilities located at each longitude between 39−41.75°N.

overlaid with the number of animal feeding operation sources along each longitude.

2.2. Instrument Overview. Full details on the TRANS^{2}Am airborne payload can be found in Juncosa Calahorrano et al.[30] Here, we use observations of gas-phase NH_3, nitric acid (HNO_3), ethene (C_2H_6), methane (CH_4), and CO, and particle-phase ammonium (NH_4^+) and nitrate (NO_3^-). Briefly, NH_3, HNO_3, and C_2H_6 were measured using individual Aerodyne Research, Inc. single-channel, quantum-cascade tunable infrared laser direct absorption spectrometers (QC-TILDAS). For the NH_3 measurements, the overall uncertainty of the instrument is ±12% of the measured mixing ratio plus a 3σ detection limit of 180 pptv.[31] For HNO_3, the instrument uncertainty is ±20% of the measured mixing ratio plus a 3σ detection limit of 555 pptv.[32] Finally, for C_2H_6, the 1 Hz precision in flight was 90 ppt, resulting in a 3σ detection limit of 270 ppt.[33] CH_4, CO, carbon dioxide (CO_2), and H_2O were measured simultaneously using a Picarro G2401-m flight-ready analyzer. Precision was 30 ppb for CO, 200 ppb for CO_2, and 2 ppb for CH_4 with low drift. Particle phase NH_4^+ and NO_3^- were measured using a Particle-into-Liquid Sampler (PILS) coupled with a fraction collector.[34] The PILS size-cut was provided by a nonrotating MOUDI impactor stage with a 50% transmission efficiency at 1 atm ambient pressure of 1 μm (PM1).[35] This system allows for the collection of liquid samples for offline analysis by ion chromatography. A Dionex ICS-3000 ion chromatograph was used to measure NH_4^+. A Dionex ICS-4000 capillary ion chromatograph was used to measure NO_3^-. The limit of detection for NH_4^+ and NO_3^- was 0.001 μg m^{-3}.

2.3. Hysplit Trajectories. We use trajectories from the Hybrid Single Particle Lagrangian Integrated Trajectory (HYSPLIT) model[36] to attribute the observed NH_3 and CH_4 plumes in L3 and L4 to a specific source location to the

https://doi.org/10.1021/acs.est.3c10902
Environ. Sci. Technol. 2024, 58, 16922−16930

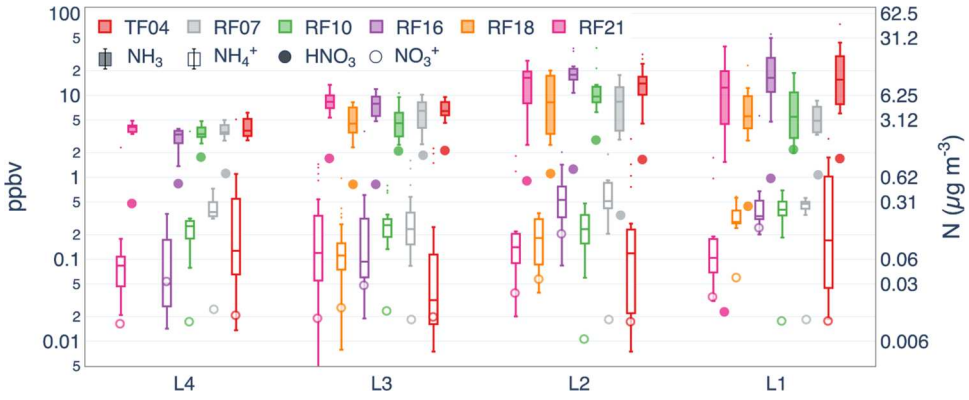

Figure 2. Distribution of 2 min averaged NH_3 (closed) and PILS NH_4^+ (open) both in ppbv (right) and $\mu g\ m^{-3}$ (left) for six upslope events sampled over Phase I and Phase II of TRANS^{2}Am. Dots represent average HNO_3 (closed) and PILS NO_3^- (open) values for that leg. L1 to L4 correspond to the transects labeled in Figure 1 and are plotted from right to left, showing the partitioning from east to west. Data includes all altitudes between the longitude ranges for each "leg" as described in Section 2.1.

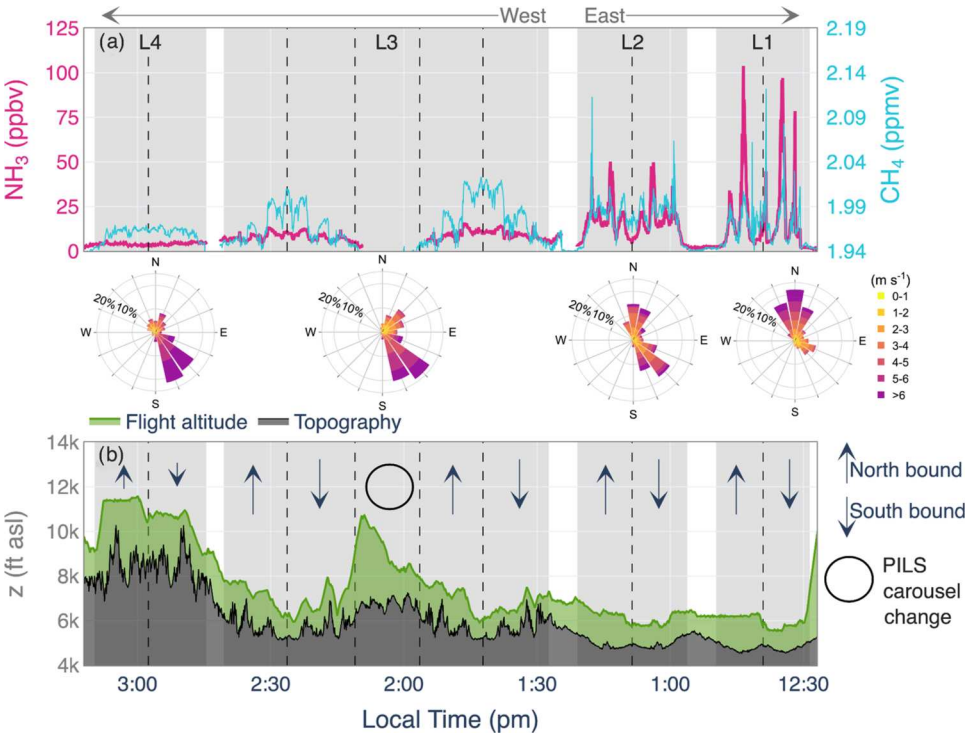

Figure 3. (a) Time series of NH_3 (pink) and CH_4 (blue) during RF21 (August 29, 2022). The *x*-axis is flipped to show the eastern legs on the right. (b) Corresponding, flying altitude (green) and topography (black). The light gray areas show the limits of each leg, excluding turns. The wind roses represent the wind observed during each sampling period.

east (e.g., animal feeding operations) and to estimate the transport time of NH_3-rich plumes from their sources to where the UWKA intercepted them along L3 and L4. We initialized ensemble sets (27 trajectories) of forward and backward trajectories using the High-Resolution Rapid Refresh (HRRR) meteorological product. The ensemble set calculates multiple trajectories in height and space, reducing the inherent uncertainties associated with running a single trajectory. Each member of the trajectory ensemble is calculated by offsetting the meteorological data by a fixed grid factor. The HRRR data set has a time step of 1 h, a 3 × 3 km^2 grid spacing, and 36σ-level layers between 1 and 0.0124. Our trajectories were initialized for a period of 6 h at the center point of sharp NH_3 enhancements within each flight leg. Each trajectory was initialized at the same altitude as the UWKA. The trajectories that contacted the surface (i.e., altitude of 0 m) were excluded from the analysis. The total distance error of the trajectories is 15−30% of the total time traveled.

3. RESULTS AND DISCUSSION

3.1. Partitioning of the Gas- and Particle-Phase NH_x.

NH_3 mixing ratios (2 min average) decrease from the eastern Colorado source region westward into the mountains, with a ∼1.5−5 (∼1.5−7)-fold reduction in the median (mean) between L1/L2 and L4 (Figure 2). Maximum 2 min NH_3 mixing ratios (1 Hz) along L1 and L2 are 74 (560) and 38 (250) ppbv, respectively. Along the westernmost legs (L3 and L4), maximum 2 min NH_3 mixing ratios (1 Hz) are 13.4 (28.2) and 6.1 (7.5) ppbv, respectively. The 2 min NH_3 10th percentiles (1 Hz) for each leg, which can be approximated to

https://doi.org/10.1021/acs.est.3c10902
Environ. Sci. Technol. 2024, 58, 16922−16930

background or out-of-plume values, are 3.2 (3.4), 3.5 (3.8), 3.3 (3.0), and 2.7 (2.8) ppbv for L1, L2, L3, and L4, respectively. Figure S2 shows 1 Hz NH_3 distributions.

NH_4^+ is more equally distributed across all the sampled legs. Mean (std) across all flights for L1, L2, L3, and L4 are 0.4 (0.6), 0.34 (0.42), 0.22 (0.35), and 0.30 (0.64) $\mu g\ m^{-3}$, respectively. A two-sided *t* test (*scipy.stats ttest_ind*) for each leg pair in each flight (36 pairs in total, 6 for each flight) indicates that the NH_4^+ means are significantly different (*p*-values <0.05) only in 7 pairs of flight legs. RF07, which was smoke-impacted, is an exception with more variability in NH_4^+. The NH_4^+ mean along L2 is significantly higher (0.623 $\mu g\ m^{-3}$) than the NH_4^+ mean along the other 3 legs (~0.3 $\mu g\ m^{-3}$) for RF07.

The difference between NH_4^+ and NH_3 abundances decreases toward the west and is largely driven by decreases in NH_3 mixing ratios. The hot and dry sampling encountered during both TRANS^{2}Am phases did not favor particle formation during the near-source flights,[32] and similar environmental conditions were present during the upslope flights. Phase I was smoke-impacted (Figure 5j–l), which is evident in the higher N-aerosol and levoglucosan concentration in L4 for Phase I (Figures S3–S4). Our observations show that in the inorganic sulfate-ammonium-nitrate system, sulfate is neutralized (free NH_3 > 0) in 100% of the observations and that the system is NH_3-rich 99.95% of the time, consistent with findings from a complementary analysis of near-source flights during Phase I of TRANS^{2}Am.[32] There is substantially more NH_4^+ (NH_3) than NO_3^- (HNO_3) in the aerosol- (gas-) phase in all the observations for the upslope events. Upslope mean total ammonium ($NH_x = NH_3 + NH_4^+$) to total nitrate ($TNO_3 = HNO_3 + NO_3^-$) ratios are 3 (10.6) on a mass (mole) basis. NH_x/TNO_3 for Phase I and II are 2 (7.5) and 4 (13.7), respectively. Reduced N dominates in the particle phase across all legs with concentrations 0.02 to 0.3 $\mu g\ m^{-3}$ higher than oxidized N. We expected to see higher percentages of TNO_3 along L3 and L4 as the aircraft is situated downwind of the urban corridor. However, *t* test analysis shows that the TNO_3 means are not different between the different legs, except for in RF16 and RF18 where TNO_3 was higher along L1 and L2 than along L3 and L4.

3.2. Plume Identification. Figure 3 shows sharp, distinct colocated plume enhancements in NH_3 and CH_4 along L1 and L2 during RF21, observed consistently across all upslope events. These enhancements differ from L3 and L4, where the NH_3 and CH_4 plume is less concentrated and broader. L1 and L2 are downwind of some of the largest animal feeding operations in the region. L1 was 2 km downwind of a large (>100,000 hd) cattle facility. However, the influences of the emissions sources along L1 on mixing ratios observed westward might be minimal given the (a) the weak easterly wind component (2–4 ms^{-1}) along L1 (see Figure 1a,b) the distance between L1 and L2 (30–32 km). L2 was located ~10 km downwind of another similarly large cattle facility (>100,000 hd).

Summertime upslope events are generally driven by differential topographic heating, characterized by low wind speeds, and upslope flow that starts near the foothills and propagates toward the plains. Since these are thermally driven events, they occur during daylight hours and are usually complemented by nighttime downslope flows.[10,18] The earlier sampling time (i.e., 12:00 and 13:00 LT) and the nature of summertime upslope flows are consistent with weaker, less organized winds observed in L1. Winds with a stronger easterly component (SE, NE, or E) were observed by the time the aircraft reached L2 (i.e., 13:00–14:00 LT). L2 and L3 are 32 km apart, which includes the narrow 12 km of the CFR urban corridor and fewer and smaller animal feeding operations (19, mostly dairies with <10,000 hd). Between L2 and L3, there is a steep decline in the NH_3 mixing ratios, explained by a combination of fewer and smaller emission sources, dilution, deposition to the ground, and/or partitioning to the particle-phase.

3.3. Variability between Upslope Events. The upslope event sampled by the UWKA on July 27, 2021 (TF04) shows strong and sustained winds (max = 9.2 ms^{-1} with gusts up to 40 ms^{-1} in L4), resulting in effective transport of NH_3 emissions westward (Figure 4). The ΔNH_3 along L1 and L2

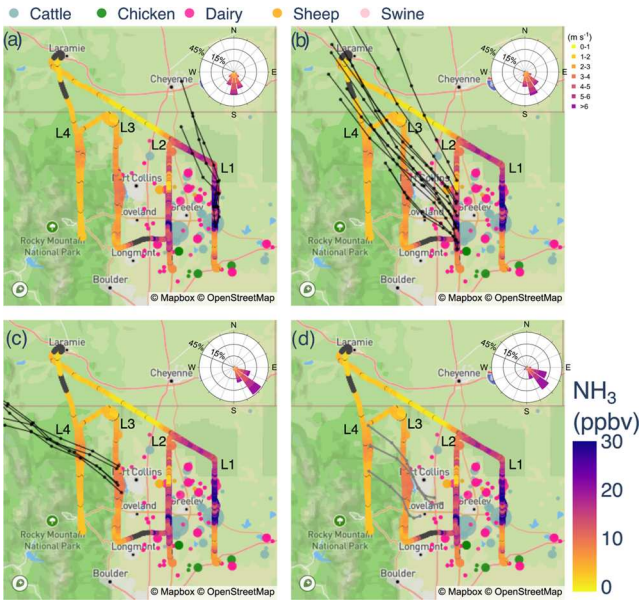

Figure 4. UWKA flight track colored by NH_3 mixing rations during TF04 (July 27, 2021). Black section along the flight plan indicates instrument zeros. The wind roses correspond to the wind observed in each leg (a–d) corresponding to L1 - L4. Circles signify livestock housing facilities colored by type of animal and sized by the reported maximum animal capacity. The black and gray lines show HYSPLIT forward and backward trajectories, respectively. Each dot within the lines represents 1 h of transport.

are large, sharp, and usually colocated near animal husbandry facilities. ΔNH_3 along L1 and L2 range between 20–550 ppbv and are colocated with ΔCH_4 of up to 600 ppbv. NH_3 along L3 and L4 reach ~10 and 7 ppbv above background (~5 and 4 ppbv), respectively. The NH_3 plume is identifiable toward the northern edge of L4, consistent with the southeasterly winds along L3.

The forward trajectories and wind roses confirm weak southerly winds that transport emissions along L1 to the north. Consistent with this picture, high NH_3 mixing ratios (up to 560 ppbv) were encountered along L1 and toward the northern portion of the UWKA flight track between L1 and L2, where no major emission sources are located. The trajectories on L1 were initialized at 11 AM LT. To investigate whether easterly flow would organize in time to transport emissions from L1 toward L2, L3, and L4, we initialized another set of forward trajectories along L1 each hour between

https://doi.org/10.1021/acs.est.3c10902
Environ. Sci. Technol. 2024, 58, 16922–16930

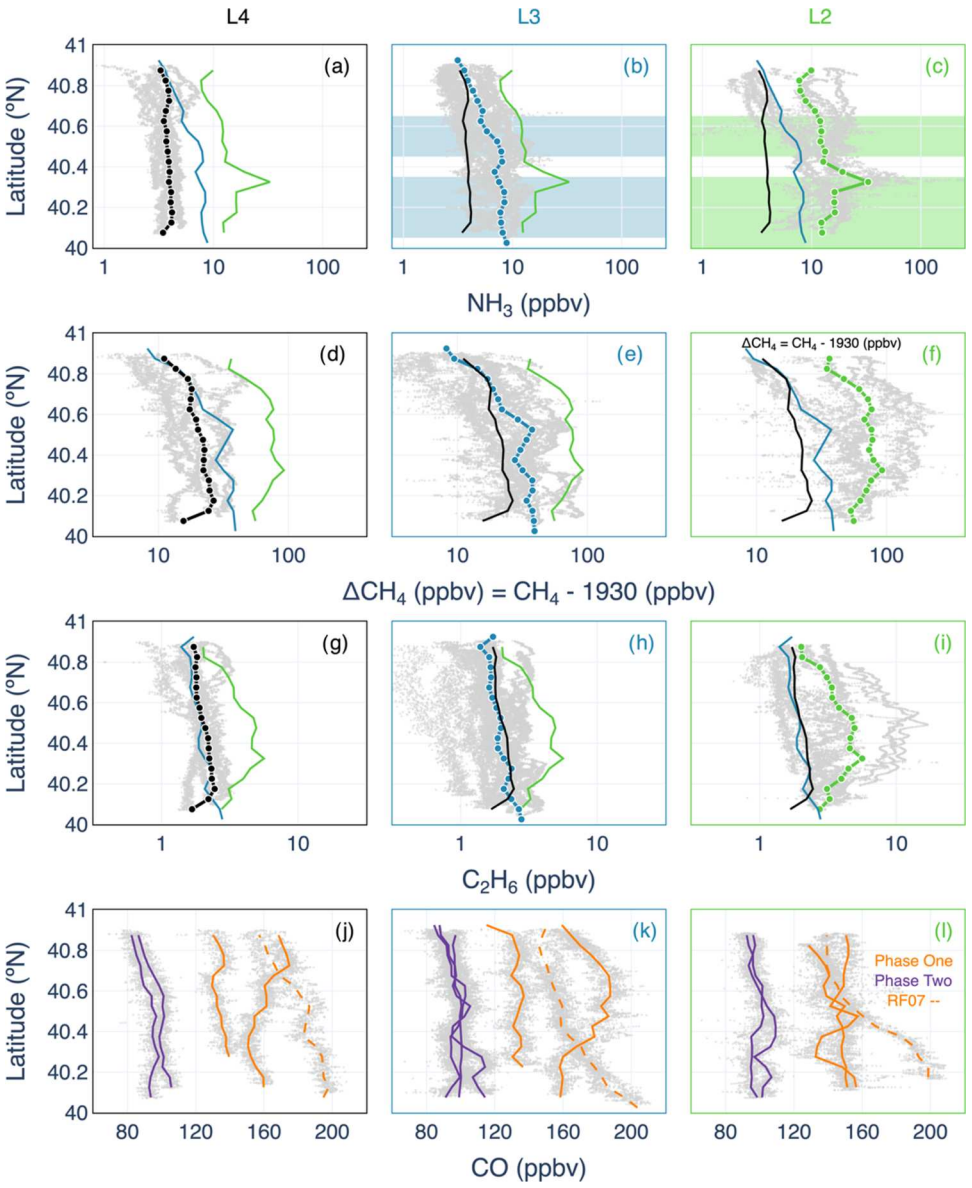

Figure 5. (a–i) 1-Hz NH_3 (top panels), ΔCH_4 (second row), C_2H_6 (third row) vs latitude binned by L4 (first column), L3 (middle column), and L2 (third column). L1 is not shown because of its unlikely contribution to the observed NH_3 enhancement along L3 and L4. Lines with circles in each panel show the latitudinal averages across that leg for all the flights. Lines with no circles show the latitudinal averages for the other two legs. Shaded regions in panels (b, c) represent the latitudes where cumulative animal capacity >100,000 animals east of the longitude of that leg. Colors remain the same across all the data (L4: black; L3: blue; and L2: green). (j–l) 1 Hz CO vs latitude binned by legs. Each line represents the latitudinal averages for CO for each flight in that leg (flights in Phase I: orange; Phase II: purple). Altitudinal average profiles are shown in Figure S9.

10 AM and 3 PM LT (not shown). The trajectories initialized after 1 PM LT suggest that plumes from emission sources along L1 could reach L2 and contribute to ΔNH_3 over the northern portion of L3 between 2 and 3 PM LT, 1–2 h after L3 was completed.

South-southeast (SSE) winds (4.4 ms^{-1}) were encountered along L2 suggesting an average transport time of 2–3 h between L2 and L3 (i.e., 30–32 km downwind) The trajectories initialized along L2 corroborate this transport time and suggest that the plume observed on L3 originates from emission sources located on the southern end of L2. Note the large NH_3 enhancements (up to 65 ppbv) near the large beef cattle facility toward the south of L2.

The trajectories initialized along L3 with predominantly southeasterly (SE) winds suggest more efficient transport into the mountains. The transport time for the plume observed along L3 to L4 is only 2 h. The trajectories suggest that the two enhancements encountered in L3 and L4 are from the same transported plume originating from the same facility along L2.

Additional upslope events (RF10, RF16, RF18, and RF21) sampled during TRANS^{2}Am show key commonalities and differences in transport efficiency of NH_3-rich plumes to the mountains (Figures S5–S8). RF16 (Figure S6) shows efficient transport of N-rich plumes to the east, similar to that of TF04 (Figure 4). RF10 and RF21 (Figures S5 and S8, respectively), show less efficient transport of plumes from major agricultural sources and the potential for recirculation of plumes to the east when they reached the mountains (i.e., L4) (see Text S2). RF18 (Figure S7), sampled earlier than other flights (11:30 AM – 3 PM) shows strong NNE winds (>10 ms^{-1}) and

https://doi.org/10.1021/acs.est.3c10902
Environ. Sci. Technol. 2024, 58, 16922–16930

efficient transport of NH_3-rich plumes toward the southernmost part of L3. L4 was not sampled during RF18 due to cloud presence. Two of the five upslope events show recirculation of polluted air to the east, whereas two suggest effective transport further west, suggesting that N-deposition in RMNP during summer could be from a recirculated and diluted plume rather or from a fresh one, depending on where the measurements are taken.

These examples show that summertime upslope events in the CFR have diverse flow patterns. A few commonalities of all the events include: (1) the largest enhancements of NH_3 and CH_4 are observed near large livestock facilities. (2) NH_3 enhancements are present over the mountains on summer afternoons when easterly winds are present in the foothills region. (3) The abundance of gas-phase NH_3 is 1 and 2 orders of magnitude higher than particle-phase NH_4^+ over the mountains and major agricultural sources, respectively.

While water treatment facilities and golf courses were not the focus of the study, L3 of our flight pattern did pass downwind of a water treatment facility and several golf courses, and we were not able to distinguish any additional NH_3 plumes. Distinguishing the contribution of vehicles on NH_3 emissions is not possible with data from Phase I of TRANS^{2}Am due to the high CO associated with the wildfire smoke. However, L3 in flights from Phase II (i.e., RF16, RF18, and RF21) have average NH_3/CO ratios of 0.26−0.55, substantially higher than vehicle emissions (0.029 ± 0.005).[37] The contribution of facilities along L1 to the NH_3 plumes observed along L3 is limited before 3 PM. The weaker and less organized winds along L1 suggest less efficient transport of emissions along L1 to the foothills (L3) and mountain (L4) legs. This is further supported by HYSPLIT trajectories that link the plumes observed along L3 to large emissions sources along L2.

3.4. NH_3 Spatial Gradient and Loss during Upslope Events. The top panels in Figure 5(a−c) show a clear regional, east-to-west gradient in NH_3 across NE CO. NH_3 mixing ratios are higher along L2, near the location of livestock facilities (e.g., 40.32°N). The average NH_3 on L2 across all sampling days ranges from 7.9−33 ppbv. Average NH_3 mixing ratios along L3 show less variability than in L2, ranging from 3.1−8.8 ppbv, with the lowest values toward the north of L3. No single peaks are observed along L3; rather, there are two broader plumes to the north and south of the peak at L2, consistent with prevailing SE or NE winds observed during TRANS^{2}Am. L4 shows the lowest and least variable NH_3 from 3.3−4.2 ppbv, with a small, broad plume toward the north of the leg.

There is also a regional east-to-west gradient in CH_4 (Figure 5d−f). A few CH_4 peaks near agricultural facilities stand out (e.g., L2:40.32°N and L3:40.52°N). Oil and gas extraction in the eastern portion of our study area, is another large source of CH_4 (see Figure S10) in the region of study, especially along L2 within the Denver-Julesburg basin. To interpret the latitudinal profiles in CH_4, we also provide latitudinal profiles of C_2H_6 (Figure 5g−i), a tracer for oil and gas activities. Both CH_4 and C_2H_6 are elevated along L2. However, there is little difference in the C_2H_6 profiles between both western legs (L3 and L4). Therefore, differences in CH_4 observed between L3 and L4 are likely attributable to the transport of agricultural emissions of CH_4 between L2 and L3 and a decreased influence from oil and gas sources between these two legs.

Based on the information in Figure 5, we use average $\Delta NH_3/\Delta CH_4$ to estimate the percentage of NH_3 loss in transport between L3 and L4. CH_4 is used as a conservative tracer since its lifetime is orders of magnitude longer than the daily transport time scales sampled in this campaign. The background values use to calculate ΔX were 3.14 ppbv and 1.938 ppmv for NH_3 and CH_4, respectively. These are the minimum values along longitudinal averages for L3 and L4. Since no agricultural (or oil and gas; see Figure S10) sources exist between L3 and L4, the difference in $\Delta NH_3/\Delta CH_4$ between these two legs is a function of the loss of NH_3 to deposition and aerosol partitioning. The $\Delta NH_3/\Delta CH_4$ (95th confidence intervals) in L3 and L4 are 0.171(±0.06) and 0.057(±0.015) ppbv ppbv^{-1}, respectively, suggesting an NH_3 loss of 67(±16)% between L3 and L4. Because upslope sampling during TRANS^{2}Am was not pseudo-Lagrangian, we need to account for the diurnal cycle in emissions from livestock facilities, which has been shown to vary significantly throughout the day.[30] On average, the plumes intercepted along L3 and L4 were emitted at 10 and 9 AM, respectively. The emission ratios of NH_3 with respect to CH_4 are estimated to be 10−30% larger at 10 AM than at 9 AM,[30] resulting in an estimated NH_3 loss of 52(±21)-63(±16)% during transport between L3 and L4. During TRANS^{2}Am, this loss is mostly in the form of dry deposition, given the absence of precipitation and low prevalence of NH_4NO_3 formation during the summertime months.[32] The same analysis for total ammonium (NH_x = NH_3 + NH_4^+), suggests that partitioning to the particle phase contributes to between 10−12.4% of the loss of gas-phase NH_3 in transit from L3 to L4. $\Delta NH_x/\Delta CH_4$ in L3 and L4 are 0.173 (±0.06) and 0.073 (±0.02) ppbv ppbv^{-1}, respectively. Correcting for the difference in emission time, this results in NH_x loss of 40(±27)-53(±21)% between L3 and L4. The formation of particle mass between L3 and L4 is further supported by an increase of 3.2 and 2.8 in $\Delta SO_4^{2-}/\Delta CH_4$ and $\Delta NO_3^-/\Delta CH_4$, respectively.

3.5. Comparison to Prior Studies in Northeastern Colorado. Several studies in Colorado have helped shape our understanding of N transport from the CFR into RMNP. The aircraft observations presented here both reinforce and challenge past findings.

During the summer, easterly winds establish close to the foothills, and their eastward extent is limited.[10] We observed this pattern in the absence of easterly flow in our easternmost flight leg. We also observed the recirculation of plumes near the mountains, which has been reported by Sullivan et al.[38] as the mountain-plains solenoid. During TRANS^{2}Am, we sampled plumes over the mountains that were likely emitted from agricultural sources in the morning. However, surface winds in Fort Collins and Greeley coupled with measurements of NH_3 in RMNP show that the stronger afternoon winds over the northern Front Range are correlated with higher NH_3 in RMNP later in the afternoon (Figures S11−S12 and Text S3), which can be partially explained by higher afternoon emissions of NH_3.[30,39]

TRANS^{2}Am observations represent agricultural plumes with excess NH_3 vs the broader range of conditions captured by the ground site in RMNP.[19] Over sites closer to the agricultural region, ∼90% of the reduced N in the atmosphere is in the gas phase,[19] which is closer to the observed partitioning during TRANS^{2}Am. Over 50% of the N measured during TRANS^{2}Am (total NO_3 and NH_4) was reduced (i.e., NH_3

https://doi.org/10.1021/acs.est.3c10902
Environ. Sci. Technol. 2024, 58, 16922−16930

and NH_4^+). NO_2 was not sampled during TRANS^{2}Am, but it is likely a large portion of the N transported to RMNP.[19]

Longitudinal averages in NH_3 across northeastern Colorado range from 3 to 33 ppbv during upslope events. Average regional gradients between the source regions and the mountains (i.e., L1) and the foothills (i.e., L2) are 10 and 7 ppbv, respectively. Passive samples collected across NE Colorado provide a consistent picture.[11,19,26] Summertime maximum regional gradients observed from 2006 to 2009[19] and 2012 to 2015[26] were ∼25 ppbv between the source region and RMNP.[26] This gradient decreased between the foothills and source region areas to ∼12 ppbv.[11] Under other wind patterns (i.e., not upslope), we expect larger differences between the westernmost legs and the source regions.

Finally, we calculate NH_3 and NH_x loss percentages (52−63 and 40−53%, respectively) between L3 and L4, which, under ideal wind conditions (sustained easterly winds) and complete information about the vertical distribution of NH_3 and CH_4, could be translated to an NH_3 deposition rate. Several studies have reported NH_3 dry deposition rates in the region between 1.8 and 27 ng NH_3 m^{-2} s^{-1},[13,19,27,28,40] with the higher values corresponding to air masses that can be traced back to the northeastern agricultural region. Our data provide useful information for future modeling efforts to further quantify the rate of NH_3 dry deposition and its latitudinal gradient in the region.

4. IMPLICATIONS AND FUTURE DIRECTIONS

The observations presented here show effective westward transport of agricultural NH_3-rich plumes from northeastern Colorado to the Rocky Mountains. Emissions from facilities near the foothills have the highest potential for efficient transport to the mountains during summer afternoons under thermally driven wind systems. We have sampled NH_3 plumes that can be largely attributed to individual livestock facilities. Future modeling efforts should benefit from considering large livestock facilities as point sources rather than area sources. Targeted reductions in emissions of NH_3 close to the foothills during summer may also be more effective in reducing summertime N-deposition under these conditions.

Due to the predominant SE winds during summer 2021 and 2022 upslope events, NH_3 deposition in the Colorado Rocky Mountains from agricultural sources likely increased from south to north during these two years. Data collected south of Berthoud, CO (and/or at 40.31°N, 105.5°W) would have under-observed agricultural NH_3 during upslope events and is likely not representative of regions to the north. Future work may include latitudinally spaced surface monitors to provide a more comprehensive constraint on N-deposition in RMNP and mountain regions to the south and north of the park.

Partitioning of NH_3 to the particle-phase was relatively minor during the warm, dry conditions characteristic of TRANS^{2}Am. However, colder and more humid conditions that occur more frequently in other seasons will promote NH_4NO_3 aerosol formation. Further, larger scale synoptically driven upslope flow, more common in spring and autumn, can push air from regions further east back up against the Rocky Mountains. Based on Li et al.[32] we expect that NH_4NO_3 formation would be a more important loss of NH_3 from October to May. Weak easterly flow is most frequent in summer for the area including Fort Collins, Greeley, and RMNP (Figure S13 and Text S4). However, stronger easterly winds often occur in spring and summer. Winter is the season with the least frequent upslope flow. A similar airborne campaign in other seasons would likely unveil important differences in (a) the partitioning of NH_3 to the particle-phase, (b) the influence of NH_3 transport from facilities located further east in the study region, and (c) additional major facilities that disproportionately contribute to NH_3 deposition in RMNP

■ ASSOCIATED CONTENT

Supporting Information

The Supporting Information is available free of charge at https://pubs.acs.org/doi/10.1021/acs.est.3c10902.

Section S1; TRANS^{2}Am upslope RF sampling strategy details (Figures S1−S2 and Text S1); Section S2; aerosol composition for upslope RF (Figures S3−S4); section S3; upslope events for RF10, RF16, RF18 and RF21 (Figures S5−S8 and Text 2); section S4; regional gradients in trace gases (Figures S9−S10); wind patterns associated with high NH_3 in RMNP (Figures 11−13 and Text S3−S4) (PDF)

■ AUTHOR INFORMATION

Corresponding Authors

Julieta F. Juncosa Calahorrano − *Department of Atmospheric Science, Colorado State University, Fort Collins, Colorado 80521, United States;* orcid.org/0000-0001-8293-7566; Email: junco004@umn.edu

Emily V. Fischer − *Department of Atmospheric Science, Colorado State University, Fort Collins, Colorado 80521, United States;* Email: emily.v.fischer@colostate.edu

Authors

Amy P. Sullivan − *Department of Atmospheric Science, Colorado State University, Fort Collins, Colorado 80521, United States*

Ilana B. Pollack − *Department of Atmospheric Science, Colorado State University, Fort Collins, Colorado 80521, United States;* orcid.org/0000-0001-7151-9756

Joseph R. Roscioli − *Aerodyne Research Inc., Billerica, Massachusetts 01821, United States*

Megan E. McCabe − *Department of Atmospheric Science, University of Wyoming, Laramie, Wyoming 82070, United States*

Kathryn M. Steinmann − *Department of Atmospheric Science, University of Wyoming, Laramie, Wyoming 82070, United States*

Dana R. Caulton − *Department of Atmospheric Science, University of Wyoming, Laramie, Wyoming 82070, United States;* orcid.org/0000-0002-5521-1871

En Li − *Department of Atmospheric Science, Colorado State University, Fort Collins, Colorado 80521, United States*

Jeffrey R. Pierce − *Department of Atmospheric Science, Colorado State University, Fort Collins, Colorado 80521, United States;* orcid.org/0000-0002-4241-838X

Lillian E. Naimie − *Department of Atmospheric Science, Colorado State University, Fort Collins, Colorado 80521, United States*

Da Pan − *Department of Atmospheric Science, Colorado State University, Fort Collins, Colorado 80521, United States;* orcid.org/0000-0002-1618-7389

Jeffrey L. Collett, Jr. − *Department of Atmospheric Science, Colorado State University, Fort Collins, Colorado 80521, United States*

Complete contact information is available at: https://pubs.acs.org/10.1021/acs.est.3c10902

Notes

The authors declare no competing financial interest.

■ ACKNOWLEDGMENTS

Funding for this work was provided by the US National Science Foundation (AGS-2020127; AGS-2020151). We wish to thank the UWKA team for their many contributions to supporting the field deployment. Thanks to Allie Mazurek and Marqi Rocque for their forecasting support during Phase I of TRANS^{2}Am. Finally, we would like to thank the two anonymous reviewers for their feedback to improve this work. Data is available in the TRANS^{2}Am data archive (https://data.eol.ucar.edu/master_lists/generated/trans2am/).

■ REFERENCES

(1) Fowler, D.; Coyle, M.; Skiba, U.; Sutton, M. A.; Cape, J. N.; Reis, S.; Sheppard, L. J.; Jenkins, A.; Grizzetti, B.; Galloway, J. N.; Vitousek, P.; Leach, A.; Bouwman, A. F.; Butterbach-Bahl, K.; Dentener, F.; Stevenson, D.; Amann, M.; Voss, M. The Global Nitrogen Cycle in the Twenty-First Century. *Philos. Trans. R. Soc., B* **2013**, *368* (1621), No. 20130164.

(2) Galloway, J. N.; Aber, J. D.; Erisman, J. W.; Seitzinger, S. P.; Howarth, R. W.; Cowling, E. B.; Cosby, B. J. The Nitrogen Cascade. *BioScience* **2003**, *53* (4), 341−356.

(3) Fenn, M. E.; Poth, M. A.; Aber, J. D.; Baron, J. S.; Bormann, B. T.; Johnson, D. W.; Lemly, A. D.; McNulty, S. G.; Ryan, D. F.; Stottlemyer, R. Nitrogen Excess In North American Ecosystems: Predisposing Factors, Ecosystem Responses, And Management Strategies. *Ecol. Appl.* **1998**, *8* (3), 706−733.

(4) Baron, J. S.; Rueth, H. M.; Wolfe, A. M.; Nydick, K. R.; Allstott, E. J.; Minear, J. T.; Moraska, B. Ecosystem Responses to NitrogeN-deposition in the Colorado Front Range. *Ecosystems* **2000**, *3* (4), 352−368.

(5) Lieb, A. M.; Darrouzet-Nardi, A.; Bowman, W. D. NitrogeN-deposition Decreases Acid Buffering Capacity of Alpine Soils in the Southern Rocky Mountains. *Geoderma* **2011**, *164* (3−4), 220−224.

(6) Wolfe, A. P.; Baron, J. S.; Cornett, R. J. Anthropogenic NitrogeN-deposition Induces Rapid Ecological Changes in Alpine Lakes of the Colorado Front Range (USA). *J. Paleolimnol.* **2001**, *25*, 1−7.

(7) Wolfe, A. P.; Van Gorp, A. C.; Baron, J. S. Recent Ecological and Biogeochemical Changes in Alpine Lakes of Rocky Mountain National Park (Colorado, USA): A Response to Anthropogenic NitrogeN-deposition. *Geobiology* **2003**, *1* (2), 153−168.

(8) Ackerman, D.; Millet, D. B.; Chen, X. Global Estimates of Inorganic NitrogeN-deposition Across Four Decades. *Global Biogeochem. Cycles* **2019**, *33* (1), 100−107.

(9) Li, Y.; Schichtel, B. A.; Walker, J. T.; Schwede, D. B.; Chen, X.; Lehmann, C. M. B.; Puchalski, M. A.; Gay, D. A.; Collett, J. L. Increasing Importance of Deposition of Reduced Nitrogen in the United States. *Proc. Natl. Acad. Sci. U.S.A.* **2016**, *113* (21), 5874−5879.

(10) Baumann, K.; Williams, E. J.; Olson, J. A.; Harder, J. W.; Fehsenfeld, F. C. Meteorological Characteristics and Spatial Extent of Upslope Events during the 1993 Tropospheric OH Photochemistry Experiment. *J. Geophys. Res.* **1997**, *102* (D5), 6199−6213.

(11) Benedict, K. B.; Carrico, C. M.; Kreidenweis, S. M.; Schichtel, B.; Malm, W. C.; Collett, J. L. A Seasonal Nitrogen-deposition Budget for Rocky Mountain National Park. *Ecol. Appl.* **2013**, *23* (5), 1156−1169.

(12) Bowman, W. D.; Murgel, J.; Blett, T.; Porter, E. Nitrogen Critical Loads for Alpine Vegetation and Soils in Rocky Mountain National Park. *J. Environ. Manage.* **2012**, *103*, 165−171.

(13) Burns, D. A. The Effects of Atmospheric NitrogeN-deposition in the Rocky Mountains of Colorado and Southern Wyoming, USA—a Critical Review. *Environ. Pollut.* **2004**, *127* (2), 257−269.

(14) Malm, W. C.; Schichtel, B. A.; Barna, M. G.; Gebhart, K. A.; Rodriguez, M. A.; Collett, J. L.; Carrico, C. M.; Benedict, K. B.; Prenni, A. J.; Kreidenweis, S. M. Aerosol Species Concentrations and Source Apportionment of Ammonia at Rocky Mountain National Park. *J. Air Waste Manage. Assoc.* **2013**, *63* (11), 1245−1263.

(15) Bowman, R. W. D.; Steltzer, H. Positive Feedbacks to Anthropogenic NitrogeN-deposition in Rocky Mountain Alpine Tundra. *Ambio* **1998**, *27* (7), 514−517.

(16) Baron, J. S. Hindcasting NitrogeN-deposition To Determine An Ecological Critical Load. *Ecol. Appl.* **2006**, *16* (2), 433−439.

(17) National Emissions Inventory (NEI). 2017 https://www.epa.gov/air-emissions-inventories/2017-national-emissions-inventory-nei-data#doc (accessed November 8, 2023).

(18) Piña, A. J.; Schumacher, R. S.; Denning, A. S.; Faulkner, W. B.; Baron, J. S.; Ham, J.; Ojima, D. S.; Collett, J. L. Reducing Wet Ammonium Deposition in Rocky Mountain National Park: The Development and Evaluation of A Pilot Early Warning System for Agricultural Operations in Eastern Colorado. *Environ. Manage.* **2019**, *64* (5), 626−639.

(19) Benedict, K. B.; Day, D.; Schwandner, F. M.; Kreidenweis, S. M.; Schichtel, B.; Malm, W. C.; Collett, J. L. Observations of Atmospheric Reactive Nitrogen Species in Rocky Mountain National Park and across Northern Colorado. *Atmos. Environ.* **2013**, *64*, 66−76.

(20) Beem, K. B.; Raja, S.; Schwandner, F. M.; Taylor, C.; Lee, T.; Sullivan, A. P.; Carrico, C. M.; McMeeking, G. R.; Day, D.; Levin, E.; Hand, J.; Kreidenweis, S. M.; Schichtel, B.; Malm, W. C.; Collett, J. L. Deposition of Reactive Nitrogen during the Rocky Mountain Airborne Nitrogen and Sulfur (RoMANS) Study. *Environ. Pollut.* **2010**, *158* (3), 862−872.

(21) Baron, J. S.; Driscoll, C. T.; Stoddard, J. L.; Richer, E. E. Empirical Critical Loads of Atmospheric NitrogeN-deposition for Nutrient Enrichment and Acidification of Sensitive US Lakes. *BioScience* **2011**, *61* (8), 602−613.

(22) Gebhart, K. A.; Schichtel, B. A.; Malm, W. C.; Barna, M. G.; Rodriguez, M. A.; Collett, J. L. Back-Trajectory-Based Source Apportionment of Airborne Sulfur and Nitrogen Concentrations at Rocky Mountain National Park, Colorado, USA. *Atmos. Environ.* **2011**, *45* (3), 621−633.

(23) Gebhart, K. A.; Malm, W. C.; Rodriguez, M. A.; Barna, M. G.; Schichtel, B. A.; Benedict, K. B.; Collett, J. L.; Carrico, C. M. Meteorological and Back Trajectory Modeling for the Rocky Mountain Atmospheric Nitrogen and Sulfur Study II. *Adv. Meteorol.* **2014**, *2014*, No. 414015.

(24) Thompson, T. M.; Rodriguez, M. A.; Barna, M. G.; Gebhart, K. A.; Hand, J. L.; Day, D. E.; Malm, W. C.; Benedict, K. B.; Collett, J. L.; Schichtel, B. A. Rocky Mountain National Park Reduced Nitrogen Source Apportionment. *J. Geophys. Res.: Atmos.* **2015**, *120* (9), 4370−4384.

(25) Schichtel, B. A.; Gebhart, K. A.; Morris, K. H.; Cheatham, J. R.; Vimont, J.; Larson, R. S.; Beachley, G. Long-term trends of wet inorganic nitrogeN-deposition in Rocky Mountain National Park: Influence of missing data imputation methods and associated uncertainty. *Sci. Total Environ.* **2019**, *687*, 817−826.

(26) Li, Y.; Thompson, T. M.; Van Damme, M.; Chen, X.; Benedict, K. B.; Shao, Y.; Day, D.; Boris, A.; Sullivan, A. P.; Ham, J.; Whitburn, S.; Clarisse, L.; Coheur, P.-F.; Collett, J. L., Jr. Temporal and Spatial Variability of Ammonia in Urban and Agricultural Regions of Northern Colorado, United States. *Atmos. Chem. Phys.* **2017**, *17* (10), 6197−6213.

(27) Benedict, K. B.; Prenni, A. J.; Sullivan, A. P.; Evanoski-Cole, A. R.; Fischer, E. V.; Callahan, S.; Sive, B. C.; Zhou, Y.; Schichtel, B. A.;

Collett, J. L., Jr Impact of Front Range Sources on Reactive Nitrogen Concentrations and Deposition in Rocky Mountain National Park. *PeerJ* **2018**, *6*, No. e4759.
(28) Pan, D.; Benedict, K. B.; Golston, L. M.; Wang, R.; Collett, J. L.; Tao, L.; Sun, K.; Guo, X.; Ham, J.; Prenni, A. J.; Schichtel, B. A.; Mikoviny, T.; Müller, M.; Wisthaler, A.; Zondlo, M. A. Ammonia Dry Deposition in an Alpine Ecosystem Traced to Agricultural Emission Hotpots. *Environ. Sci. Technol.* **2021**, *55* (12), 7776−7785.
(29) National Center for Environmental Information. Annual 2021 Wildfires Report, 2023 https://www.ncei.noaa.gov/access/monitoring/wildfires/ (accessed September 29, 2023).
(30) Juncosa Calahorrano, J. F.; Pollack, I. B.; Sullivan, A. P.; Roscioli, J. R.; Caulton, D. R.; McCabe, M. E.; Li, E.; Pierce, J. R.; Fischer, E. V. Summertime Airborne Measurements of Ammonia Emissions From Cattle Feedlots and Dairies in Northeastern Colorado. *J. Geophys. Res.: Atmos.* **2023**, *128* (23), No. e2023JD039043.
(31) Pollack, I. B.; McCabe, M. E.; Caulton, D. R.; Fischer, E. V. Enhancements in Ammonia and Methane from Agricultural Sources in the Northeastern Colorado Front Range Using Observations from a Small Research Aircraft. *Environ. Sci. Technol.* **2022**, *56* (4), 2236−2247.
(32) Li, E.; Pierce, J. R.; Juncosa Calahorrano, J. F.; Sullivan, A. P.; Pollack, I. B.; Roscioli, J. R.; Caulton, D. R.; McCabe, M. E.; Jathar, S. H.; Fischer, E. V. Inorganic Nitrogen Gas-Aerosol Partitioning in and around Animal Feeding Operations in Northeastern Colorado in Late Summer 2021. *J. Geophys. Res.: Atmos.* **2024**, *129*, No. e2023JD040507.
(33) McCabe, M. E.; Pollack, I. B.; Fischer, E. V.; Steinmann, K. M.; Caulton, D. R. Technical Note: Isolating Methane Emissions from Animal Feeding Operations in an Interfering Location. *Atmos. Chem. Phys.* **2023**, *23* (13), 7479−7494.
(34) Sullivan, A. P.; Pokhrel, R. P.; Shen, Y.; Murphy, S. M.; Toohey, D. W.; Campos, T.; Lindaas, J.; Fischer, E. V.; Collett, J. L., Jr. Examination of Brown Carbon Absorption from Wildfires in the Western US during the WE-CAN Study. *Atmos. Chem. Phys.* **2022**, *22* (20), 13389−13406.
(35) Marple, V. A.; Rubow, K. L.; Behm, S. M. A Microorifice Uniform Deposit Impactor (MOUDI): Description, Calibration, and Use. *Aerosol Sci. Technol.* **1991**, *14* (4), 434−446.
(36) Draxler, R. R.; Hess, G. D. An overview of the HYSPLIT_4 modeling system of trajectories, dispersion, and deposition. *Aust. Meteorol. Mag.* **1998**, *47*, 295−308.
(37) Sun, K.; Tao, L.; Miller, D. J.; Pan, D.; Golston, L. M.; Zondlo, M. A.; Griffin, R. J.; Wallace, H. W.; Leong, Y. J.; Yang, M. M.; et al. Vehicle emissions as an important urban ammonia source in the United States and China. *Environ. Sci. Technol.* **2017**, *51*, 2472−2481.
(38) Sullivan, J. T.; McGee, T. J.; Langford, A. O.; Alvarez, R. J.; Senff, C. J.; Reddy, P. J.; Thompson, A. M.; Twigg, L. W.; Sumnicht, G. K.; Lee, P.; Weinheimer, A.; Knote, C.; Long, R. W.; Hoff, R. M. Quantifying the Contribution of Thermally Driven Recirculation to a High-Ozone Event along the Colorado Front Range Using Lidar: O_3 Lidar During Recirculation Event. *J. Geophys. Res.: Atmos.* **2016**, *121* (17), 10377−10390.
(39) Eilerman, S. J.; Peischl, J.; Neuman, J. A.; Ryerson, T. B.; Aikin, K. C.; Holloway, M. W.; Zondlo, M. A.; Golston, L. M.; Pan, D.; Floerchinger, C.; Herndon, S. Characterization of Ammonia, Methane, and Nitrous Oxide Emissions from Concentrated Animal Feeding Operations in Northeastern Colorado. *Environ. Sci. Technol.* **2016**, *50* (20), 10885−10893.
(40) Campbell, P. C.; Tong, D.; Saylor, R.; Li, Y.; Ma, S.; Zhang, X.; Kondragunta, S.; Li, F. Pronounced Increases in Nitrogen Emissions and Deposition Due to the Historic 2020 Wildfires in the Western U.S. *Sci. Total Environ.* **2022**, *839*, No. 156130.

https://doi.org/10.1021/acs.est.3c10902
Environ. Sci. Technol. 2024, 58, 16922−16930